ChemComm

COMMUNICATION

View Article Online
View Journal | View Issue

Cite this: *Chem. Commun.*, 2016, 52, 13357

Received 12th August 2016,
Accepted 12th October 2016

DOI: 10.1039/c6cc06629a

www.rsc.org/chemcomm

Efficient electro/photocatalytic water reduction using a $[Ni^{II}(N_2Py_3)]^{2+}$ complex†

Pavithra H. A. Kankanamalage, Shivnath Mazumder,‡ Vishwas Tiwari, Kenneth K. Kpogo, H. Bernhard Schlegel and Cláudio N. Verani*

The pyridine-rich complex $[Ni^{II}(L^{N_2Py_3})(MeCN)](ClO_4)_2$ (1) acts as an efficient electro- and photocatalyst in the generation of H_2 from water. Observed TONs reach 1050 for electrocatalysis and a remarkable 3500 for photocatalysis. Experimental and DFT data support the ligand-reduced $[Ni^{I}L^{\bullet}]$ as the catalytically active species, contrasting with the $[Co^{I}L]$ observed for cobalt catalysts.

Limited fossil fuel reserves and excessive CO_2 emission require an urgent search for renewable energy sources.[1] Dihydrogen is an ideal candidate due to its high energy density and the formation of water as the sole combustion product.[2] Cobalt complexes have been extensively studied for H_2 production because of the energetically affordable conversions from $3d^6$ Co^{III} to $3d^7$ Co^{II} to $3d^8$ Co^{I} species.[3] Other abundant metal ions like the $3d^6$ Fe^{II}, $3d^8$ Ni^{II}, and $3d^9$ Cu^{II} have been considerably less studied despite their potential as new electrocatalysts and photocatalysts. Nickel is particularly relevant because of its role in the active site of hydrogenases involved in the splitting of H_2 into two H^+.[4] The Bullock/Dubois catalyst is thus far the best nickel-based molecular electrocatalyst in organic media.[5] However, reliance on DMF and dry acetonitrile makes this an expensive approach. Other ligand systems such as N_4-macrocyclic,[6] oxime,[7] and pyridine/thiolate,[8] and pincer[9] complexes have shown promise towards catalysis, in spite of ligand involvement in proton transfer. Similarly, some pyridine-based systems have been evaluated but their full potential as photocatalysts is yet to be realized.[10] Based on our current knowledge of cobalt chemistry and on a ligand framework recognized for good turnover numbers (TONs) in water,[3] we hypothesize that replacing cobalt with nickel will lead to new and effective catalysts. These pyridine-containing compounds enable the investigation of issues related to electrocatalytic and photocatalytic activity, while allowing for mechanistic comparisons between nickel and cobalt catalysts in similar environments. It is currently accepted that Ni will undergo a mechanism similar to that of Co catalysts,[9,10b,11] following reduction from Ni^{II} to Ni^{I}, then transferring $2e^-$ to a H^+ to form a Ni^{III}–H^- species, and finally interacting with another H^+ to yield H_2, thus regenerating the Ni^{II} catalyst. Alternatively, it has been proposed that the pyridine ligand may be reduced to form a bivalent $[Ni^{II}L^{\bullet}]$ species. Both mechanisms require the formation of Ni^{III} as the hydride bearer, and alternatively, ligand reduction is equally acceptable: $[Ni^{II}L] \rightarrow [Ni^{I}L] \rightarrow [Ni^{I}L^{\bullet}]$. This species will then generate a Ni^{II}–H^- species that might be thermodynamically more affordable than a trivalent species. In this paper we present a new complex $[Ni^{II}(L^{N_2Py_3})(MeCN)](ClO_4)_2$ (**1**) (Fig. 1) and (i) evaluate its electrocatalytic activity in MeCN and water at pH 7, (ii) evaluate its photocatalytic activity in 1 : 1 water/EtOH in the pH range of 10 to 14, including the role of the photosensitizer, and (iii) propose a new mechanism associated with H_2 generation.

The ligand $L^{N_2Py_3}$ was synthesized as previously described[3] and then treated with $[Ni^{II}(H_2O)_6](ClO_4)_2$ in methanol (MeOH). A pink precipitate was filtered and recrystallized in 1 : 1 MeOH : MeCN to yield X-ray quality crystals of $[Ni^{II}(L^{N_2Py_3})(MeCN)](ClO_4)_2$ (**1**). The nature of **1** was confirmed by elemental analysis and ESI mass analysis. The NMR spectrum of **1** displayed broad solvent peaks, confirming the presence of a high spin Ni^{II} ion. The structure obtained by X-ray diffraction shows a six-coordinate Ni^{II} cationic complex with pseudo-octahedral geometry (Fig. 1) where three pyridine (N_{Py}) atoms N3, N4, and N5, and the methylated tertiary N1 form the basal plane, with the non-methylated tertiary amine

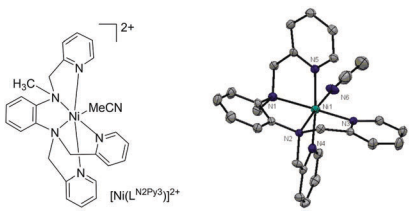

Fig. 1 The cation $[Ni^{II}(L^{N_2Py_3})(MeCN)]^{2+}$ of **1** and its ORTEP at 50% probability. H atoms and counterions are omitted. CCDC 1492143.

Department of Chemistry, Wayne State University, 5101 Cass Ave., Detroit, MI 48202, USA. E-mail: cnverani@chem.wayne.edu

† Electronic supplementary information (ESI) available: Comprehensive experimental and theoretical information. CCDC 1492143. For ESI and crystallographic data in CIF or other electronic format see DOI: 10.1039/c6cc06629a

‡ Current address: Chemistry Department, Hofstra University, Hempstead, NY 11549, USA.

N2 perpendicular to the plane. The sixth position is occupied by a molecule of acetonitrile *trans* to the non-methylated tertiary amine.

The six Ni–N bonds vary from 2.024(4) to 2.114(3) Å, consistent with reported Ni^{II} complexes.[12] Detailed bond lengths and crystallographic parameters are summarized in Tables ST1, ST2, and ST3 (ESI†). The Ni–N6–C25 (MeCN) bond angle is 168.6(4)° and the Ni–N_{MeCN} bond distance is 2.028(3) Å. The Ni–N_{MeCN} bond length is shorter than other reported apical acetonitrile ligands,[12] likely being of importance to the dissociation of the axial ligand that provides an open coordination site for protons to bind to the Ni center during catalysis.

The electronic absorption spectrum of **1** was recorded in MeCN (Fig. S1, ESI†). Similar to the free ligand, the complex shows pronounced bands at 260 nm ($\varepsilon \approx 10\,200\ M^{-1}\ cm^{-1}$) and 302 nm ($\varepsilon \approx 270\ M^{-1}\ cm^{-1}$) due to intraligand charge transfers (CT). While no obvious metal/ligand CT bands are observed, three low-intensity d–d bands are found at 520, 810, and 880 nm ($\varepsilon \approx 18\ M^{-1}\ cm^{-1}$ for all three) and, respectively, associated with the transitions $^3T_2 \leftarrow {}^3A_2$, $^3T_1(F) \leftarrow {}^3A_2$, and $^3T_1(P) \leftarrow {}^3A_2$ of an approximate octahedral ligand field.[13] The redox behavior of **1** was determined by cyclic voltammetry (CV) in MeCN and three redox processes were observed (Fig. S2, Tables ST4 and ST5, ESI†). The first oxidation at $E_{1/2}$ = 1390 $mV_{Fc/Fc+}$ is tentatively attributed to the Ni^{II}/Ni^{III} couple.[10a] The reduction wave observed at −1830 $mV_{Fc/Fc+}$ is attributed to the Ni^{II}/Ni^{I} couple, while that at −2140 $mV_{Fc/Fc+}$ is a ligand-based reduction. DFT calculations[14] support that the first irreversible reduction is a $3d^8$ Ni^{II} to $3d^9$ Ni^{I} metal-based event, while the second reduction leads to a $[Ni^{I}L^{\bullet}]$ species. Lack of NMR data and DFT calculations support the $3d^8$ Ni^{II} center in **1** as a high-spin triplet with half-filled $\left(d^1_{x^2-y^2}d^1_{z^2}\right)$ e_g-like MOs. The electronic spectrum of the $1e^-$ reduced $\mathbf{1}^-$ (Fig. S3, ESI†) confirms these attributions with the appearance of a band at 560 nm associated with a weak $L_{\pi^*} \leftarrow Ni^{I}_{\left(d_{x^2-y^2}\right)}$ MLCT, and another band at *ca.* 1000 nm likely associated with red-shifted d_{xz}, $d_{yz} \leftarrow d_{xy}$ transitions[15] or a $Ni^{I}_{d_{x^2-y^2}} \leftarrow L_{\pi^*}$ LMCT, thus suggesting a $[Ni^{II}L^{\bullet}]$ character. The related EPR spectrum (Fig. S4, ESI†) supports a genuine Ni^{I} species[16] and DFT calculations do not converge onto a ligand radical species in this case. The spectrum of a $2e^-$ reduced $\mathbf{1}^{-2}$ sees further increase of the first band and maintenance of the second.

In order to probe catalytic H_2 generation by **1**, a CV experiment was performed in MeCN using 0 to 20 equivalents of acetic acid as the proton source (Fig. 2 and Fig. S5a, ESI†).

The reduction at −2140 $mV_{Fc/Fc+}$ yields the ligand-reduced $[Ni^{I}L^{\bullet}]$ species and the corresponding catalytic peak increases with an increasing concentration of acid equivalents, suggesting that this is the catalytically active species. Control experiments confirm the need for catalyst **1** (Fig. S5b, ESI†). To demonstrate that the catalytic peak observed in the CV is due to H_2 production, a bulk electrolysis (BE) experiment was performed at an applied potential of −1700 $mV_{Ag/AgCl}$ in MeCN. Following the addition of 100 equivalents of acid, a TON of 8 with a Faradaic efficiency (FE) of 55% was calculated after 3 h (Fig. 2, inset). These results suggest that **1** is only a moderate catalyst in organic medium.

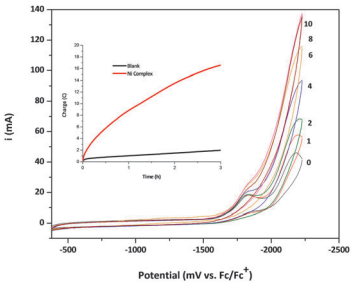

Fig. 2 CVs of **1** in MeCN, $TBAPF_6$ (0.1 M) with 0–10 equiv. of acid. Electrodes: C_{glassy} (W), Ag/AgCl (R), Pt wire (A). Inset: Charge *vs.* time plot for 3 h BE; 5.0 μmol of **1** at −1700 $mV_{Ag/AgCl}$. Electrodes: Hg pool (W), Ag/AgCl (R), Pt wire (A).

To test the viability of **1** as a potential water reduction catalyst, a CV experiment was performed in phosphate buffer (1 M, pH 7) using a mercury pool working electrode. In the absence of **1**, generation of H_2 by the electrode was observed at a potential of −1850 $mV_{Ag/AgCl}$. This peak shifted to a considerably more positive potential of −1450 $mV_{Ag/AgCl}$ in the presence of **1** (Fig. 3a), thus indicating its catalytic activity towards water reduction. The onset overpotential was calculated at 833 mV (the thermodynamic potential for H^+ to H_2 was taken as −617 $mV_{Ag/AgCl}$ in pH 7 aqueous solution).[2] Precise confirmation of the value for the onset overpotential came from BE in phosphate buffer (1 M, pH 7) in which the applied overpotentials were varied every 3 min from 180 mV to 930 mV. The experiment revealed that only negligible charge consumption is observed below 780 mV (Fig. 3b).

To confirm that the catalytic peak (Fig. 3a) observed in the presence of **1** (7 μmol L^{-1}) is associated with water reduction, BE was performed at −1700 $mV_{Ag/AgCl}$ in phosphate buffer (1 M, pH 7) and the gas produced inside the cell headspace was collected and analyzed by gas chromatography. Under these conditions **1** produced a TON of 1050 (TOF = 350 h^{-1}) with a FE of 96% after 3 h. Prolonged electrocatalysis of 18 h (Fig. S6, ESI†) yielded a TON no greater than 2000–2500 with a considerable decrease of FE to about 35%. Dihydrogen produced continuously over 18 h BE helped determine the dependence of the TON and TOF on time. Fig. S7a (ESI†) shows that the TON does not increase linearly with time; rather, **1** catalyzes H_2 production at the maximal rate up to 3 to 5 h before the plot of TON *vs.* time shows a considerable decrease in slope. The TOF started decreasing after 3 h. UV-visible absorption spectra were

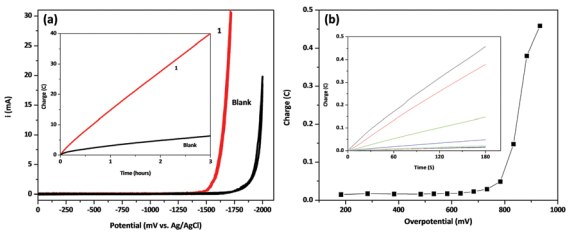

Fig. 3 (a) CV of **1** in water (pH 7, 1M phosphate buffer). Inset: Charge *vs.* time plot for 3 h BE at −1700 $mV_{Ag/AgCl}$. (b) Charge *vs.* overpotential plot at various overpotentials over 3 min intervals. Inset: Charge accumulation (3 min.) *vs.* time plot; 0.1 μmol of **1**. Electrodes: Hg pool (W), Ag/AgCl (R), Pt wire (A).

recorded before and after catalysis to understand the fate of the catalyst (Fig. S7b, ESI†). A tenfold higher concentration of **1** (70 μmol L^{-1}) was required to provide a more detailed spectrum but the absence of metal/ligand CT bands makes the analysis difficult. After catalysis, the initial intraligand bands around 260 nm diminished and new, less intense bands at 246 and 294 nm were observed.

Changes in pre- and post-catalysis spectra allied to the changes in TON and TOF suggest the conversion of the catalyst into a chemically different and inactive species. The likely processes may involve (i) substitution of the axial MeCN ligand by water at the closing of the catalytic cycle, (ii) possible formation of nanoparticulates, or (iii) deleterious ligand degradation that leads to catalyst deactivation. To verify these hypotheses, MeCN was added to a post-catalytic solution of phosphate buffer in a 1 : 1 ratio and stored at −18 °C for 24 h. The water freezes and the phosphate salts crash out, allowing for recovery of the remaining MeCN layer. The resulting UV-visible spectrum in Fig. S8 (ESI†) shows decreased intensity and is similar to that of the post-catalytic complex in phosphate buffer, thereby ruling out ligand exchange as a source of variation. The formation of nanoparticles was studied by BE experiments in phosphate buffer (1 M, pH 7) using Grafoil® as the working electrode. The scanning electron microscopy (SEM) images of this electrode are shown in Fig. S9 (ESI†), where the formation of solid particles is evident. However, energy dispersive spectroscopy (EDS) analysis indicates that nickel is absent in these particles (Tables ST5 and ST6, ESI†). Thus the SEM images and EDS analysis support the existence of a molecular Ni catalyst, even after 8 h of BE, indicating that its deactivation must take place through some other mechanism, likely involving ligand degradation.

If formation of the hydride species involved ligand reduction, then formation of organic radicals might be a possible deactivation mechanism. In order to evaluate this possibility we used DFT-calculations to evaluate the electrocatalytic mechanism of H_2 generation by **1**, as shown in Fig. 4. In water, the MeCN in **1** is readily displaced by H_2O. Reduction of $[Ni^{II}(L^{N_2Py_3})(H_2O)]^{2+}$ yields a five-coordinate $3d^9$ species **A**, $[Ni^{I}(L^{N_2Py_3})(H_2O)]^{+}$, which has lost the coordination of a pyridine. Loss of H_2O from this five-coordinate species is then favorable by 7.2 kcal mol^{-1}. This leads to the formation of $[Ni^{I}(L^{N_2Py_3})]^{+}$ (**B**) that is equally five-coordinate due to re-coordination of the pendant pyridine. This $3d^9$ Ni^{I} complex can undergo a second one-electron reduction at −2260 $mV_{Fc/Fc+}$, yielding the ligand-reduced and radical-bearing $[Ni^{I}(L^{N_2Py_3\bullet})]^{0}$ species (**C**) where the unpaired electron on the $3d^9$ Ni^{I} couples antiferromagnetically to the pyridine moiety resulting in an overall singlet ($S = 0$) spin state (Fig. S10a, ESI†). This step is relevant because it favors ligand reduction rather than a second metal-centered reduction that would lead to a metal-based Ni^{0} species, found to be 7.5 kcal mol^{-1} higher in energy. This Ni^{0} species would have a severely distorted coordination sphere where three of the Ni–N bonds are considerably elongated and would likely trigger catalyst degradation. Addition of a proton to the doubly-reduced **C** leads to the formation of a $3d^8$ Ni^{II}–H^- hydride intermediate $[(L^{N_2Py_3})Ni^{II}–H]^{+}$ (**D**); this event is significantly favorable by 59 kcal mol^{-1}, suggesting that **C** is catalytically relevant. In contrast, protonation of the singly-reduced **B** requires formation

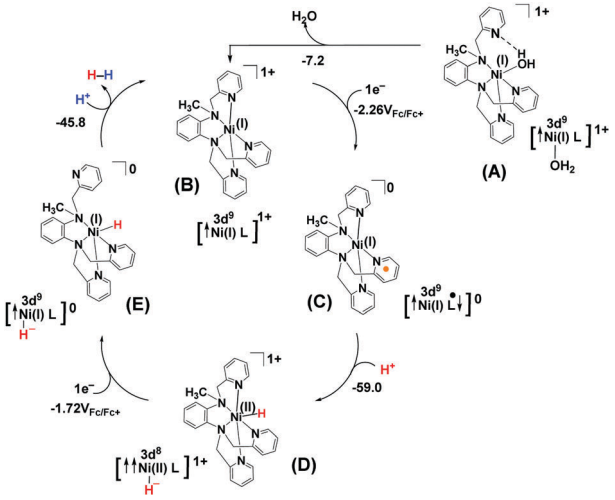

Fig. 4 The electrocatalytic mechanism of H_2 generation by **1** in H_2O. The free energies (kcal mol^{-1}) and potentials (in volts) have been calculated at the B3LYP/SDD/6-31G(d,p) level of theory.[18]

of a trivalent $3d^7$ $[Ni^{III}–H^-]$ complex that is isoenergetic with **B** (+0.2 kcal mol^{-1}, Fig. S11, ESI,† structure F); however, this protonation becomes energetically even less favorable at higher pH. Thus, considering the favorability of the $3d^8$ Ni^{II} hydride, this $3d^7$ Ni^{III} hydride is significantly less catalytically relevant. This observation contrasts with the mechanism proposed for similar water-reducing cobalt catalysts.[3,17]

Here, the pyridine-rich ligand framework shows redox non-innocent behavior and acts as an electron reservoir to avoid formation of the high energy trivalent intermediate. The Ni^{II}–H^- intermediate **D** can undergo another one-electron reduction at −1720 $mV_{Fc/Fc+}$ to form the five-coordinate Ni^{I}–H^- complex **E**. Uptake of a proton by the latter species evolves H_2 and the resulting $[Ni^{I}(L^{N_2Py_3})]^{+}$ complex **B** can reenter the catalytic cycle. This event is favorable by 46 kcal mol^{-1}. In contrast, H_2 evolution from **D** is favorable by only 33 kcal mol^{-1}. An alternative pathway is proposed in Fig. S12 (ESI†), involving H_2O coordinated to a square planar Ni. Formation of a Ni^{I}(OH) species is proposed in order to initiate deleterious catalyst deactivation in water (Fig. S13, ESI†). Furthermore, the ligand-reduced $[Ni^{I}(L^{N_2Py_3\bullet})]^{+}$ species **C** is also likely to contribute to catalyst deactivation. The ultimate goal of a water reduction catalyst is the generation of H_2 from water using light as the sole energy source. Because fluorescein (Fl) and green light (520 nm) have been used as photosensitizers with Ni complexes for H_2 generation,[8] the photocatalytic activity of **1** was also tested under similar conditions. A TON of 716 was achieved for **1** (30 μM) in water/EtOH (1 : 1) at pH 12 using triethylamine (TEA, 5% v/v) as the sacrificial electron donor and Fl (1 mM) for 24 h.

The catalytic activity was evaluated by varying the electron donor to find out which species worked best with the **1**/Fl system. Besides TEA, triethanolamine (TEOA) was also used at pH 12, and ascorbic acid (AA) was used at pH values of 5 and 12. Systems with TEOA and AA did not generate H_2 under the given conditions, suggesting that TEA is a superior electron donor candidate.

The dependence of TON on pH was tested by varying the pH of the medium (Fig. 5a). Previous reports on photocatalytic

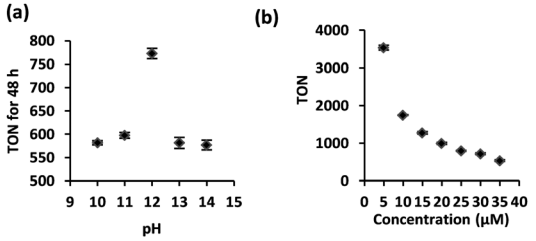

Fig. 5 (a) Variation of the TON with the pH of the photocatalytic systems containing **1** (30 μM), Fl (1 mM), and TEA (5% v/v) in EtOH/water (1 : 1). (b) Variation of the TON with concentration of **1** at pH 12, in Fl (1 mM) and TEA (5% v/v) in the EtOH/water (1 : 1) system.

systems have suggested that TEA can perform better as an electron donor, when at higher pH values;[8a] thus experimental variations from pH 10 to 14 revealed optimal performance at pH 12. Photocatalytic dependence on the photosensitizer was also investigated by changing Fl with $[Ru(bpy)_3]^{2+}$ (1 mM). Illumination with blue light (480 nm) in the presence of **1** (30 μM) and TEA (5% v/v) for 24 h gave a TON of 174. Therefore, under the same conditions, Fl is more effective than $[Ru(bpy)_3]^{2+}$ in the generation of H_2. The impact of the electron donor on $[Ru(bpy)_3]^{2+}$ was also considered by changing TEA with TEOA at pH 12, as well as AA at pHs of 5 and 12. Again, only TEA was able to produce H_2 with $[Ru(bpy)_3]^{2+}$. The influence of the concentration of **1** on photocatalysis was monitored with Fl (1 mM) and TEA (5% v/v) in water/EtOH (1 : 1) at pH 12 (Fig. 5b). The concentration of **1** was varied from 5 to 35 μM, and under these conditions, the catalyst concentration and TON vary inversely; a maximum TON of 3500 was found after 24 h for the system with the lowest concentration (5 μM) of the Ni catalyst. The TON of **1** (5 μM) in the presence of Fl (1 mM) and TEA (5% v/v) in EtOH/water (1 : 1) remained constant upon addition of *ca.* 1 mL of Hg to the reaction vessel, indicating that formation of metal colloids is not responsible for H_2 production (Table ST7, ESI†).[19] Furthermore, tunneling electron microscopy (TEM) images were taken by adding a few drops of the photocatalytic mixture in the presence and absence (blank) of **1** (Fig. S14, ESI†). The TEM images of both mixtures feature small solid particles; however, EDS analysis confirms that Ni particulates are below the detection threshold (Table ST8, ESI†), suggesting the absence of colloidal matter.

In conclusion, we introduced a new nickel-based complex $[Ni^{II}(L^{N_2Py_3})(MeCN)](ClO_4)_2$ (**1**) that has been synthesized and thoroughly characterized. This complex is active both as an electrocatalyst and as a photocatalyst. Water reduction by **1** at pH 7 and an onset potential of 780 mV yielded a TON of 1050 after 3 h. In stark contrast, a TON of 3500 was measured for photocatalytic water reduction by **1** in the presence of fluorescein and TEA at pH 12. We propose that the electrocatalytic mechanism of H_2 generation involves a $3d^9$ Ni^I intermediate in which the ligand is further reduced to form a $[Ni^I(L^\bullet)]^0$ species that, upon addition of a proton, yields the highly favorable Ni^{II}–H^- complex, thus avoiding formation of the trivalent Ni^{III}–H^- congener. The post-catalytic fate of **1** seems to include deactivation *via* radical mechanisms, but formation of nanoparticulates is unlikely. It is noteworthy that the same ligand involvement that precludes formation of the trivalent nickel hydride species is also associated with the deactivation of the molecular catalyst. Therefore efforts towards improving the efficiency of such catalysts must find a balance between these two extreme situations. Robust ligand frameworks capable of withstanding multiple catalytic cycles will be necessary to enable water reduction with nickel catalysts.

This work was supported by the U.S. Department of Energy, Office of Science, Office of Basic Energy Sciences, under award DE-SC0001907 (to C. N. V. and H. B. S.). V. T. is a Chemistry undergraduate student and acknowledges a WSU-Presidential Scholarship.

Notes and references

1 N. S. Lewis and D. G. Nocera, *Proc. Natl. Acad. Sci. U. S. A.*, 2006, **103**, 15729.
2 (*a*) V. S. Thoi, Y. Sun, J. R. Long and C. J. Chang, *Chem. Soc. Rev.*, 2013, **42**, 2388; (*b*) M. Wang, L. Chen and L. Sun, *Energy Environ. Sci.*, 2012, **5**, 6763.
3 (*a*) D. Basu, S. Mazumder, X. Shi, H. Baydoun, J. Niklas, O. Poluektov, H. B. Schlegel and C. N. Verani, *Angew. Chem.*, 2015, **127**, 2133; (*b*) L. Tong, R. Zong and R. P. Thummel, *J. Am. Chem. Soc.*, 2014, **136**, 4881; (*c*) W. M. Singh, T. Baine, S. Kudo, S. Tian, X. A. Ma, H. Zhou, N. J. DeYonker, T. C. Pham, J. C. Bollinger, D. L. Baker, B. Yan, C. E. Webster and X. Zhao, *Angew. Chem., Int. Ed.*, 2012, **51**, 5941.
4 W. Lubitz, H. Ogata, O. Rüdiger and E. Reijerse, *Chem. Rev.*, 2014, **114**, 4081.
5 M. L. Helm, M. P. Stewart, R. M. Bullock, M. R. DuBois and D. L. DuBois, *Science*, 2011, **333**, 863.
6 J. P. Collin, A. Jouaiti and J. P. Sauvage, *Inorg. Chem.*, 1988, **27**, 1986.
7 O. Pantani, E. Anxolabéhère-Mallart, A. Aukauloo and P. Millet, *Electrochem. Commun.*, 2007, **9**, 54.
8 Z. Han, L. Shen, W. W. Brennessel, P. L. Holland and R. Eisenberg, *J. Am. Chem. Soc.*, 2013, **135**, 14659.
9 O. R. Luca, J. D. Blakemore, S. J. Konezny, J. M. Praetorius, T. J. Schmeier, G. B. Hunsinger, V. S. Batista, G. W. Brudvig, N. Hazari and R. H. Crabtree, *Inorg. Chem.*, 2012, **51**, 8704.
10 (*a*) A. Call, Z. Codolà, F. Acuña-Parés and J. Lloret-Fillol, *Chem. – Eur. J.*, 2014, **20**, 6171; (*b*) P. Zhang, M. Wang, Y. Yang, D. Zheng, K. Han and L. Sun, *Chem. Commun.*, 2014, **50**, 14153; (*c*) R. Tatematsu, T. Inomata, T. Ozawa and H. Masuda, *Angew. Chem.*, 2016, **55**, 5247.
11 J. Han, W. Zhang, T. Zhou, X. Wang and R. Xu, *RSC Adv.*, 2012, **2**, 8293.
12 O. R. Luca, S. J. Konezny, J. D. Blakemore, D. M. Colosi, S. Saha, G. W. Brudvig, V. S. Batista and R. H. Crabtree, *New J. Chem.*, 2012, **36**, 1149.
13 B. N. Figgis and M. A. Hitchman, *Ligand field theory and its applications*, Wiley-VCH, New York, 2000.
14 M. J. Frisch, G. W. Trucks and H. B. Schlegel, *et al.* Gaussian 09, Revision E. 01, Gaussian, Wallingford, CT, USA, 2013.
15 (*a*) S. V. Kryatov, B. S. Mohanraj, V. V. Tarasov, O. P. Kryatova, E. V. Rybak-Akimova, B. Nuthakki, J. F. Rusling, R. J. Staples and A. Y. Nazarenko, *Inorg. Chem.*, 2002, **41**, 923; (*b*) M. Valente, C. Freire and B. de Castro, *J. Chem. Soc., Dalton Trans.*, 1998, 1557.
16 R. R. Gagne and D. M. Ingle, *Inorg. Chem.*, 1981, **20**, 420.
17 (*a*) D. Basu, S. Mazumder, X. Shi, R. J. Staples, H. B. Schlegel and C. N. Verani, *Angew. Chem., Int. Ed.*, 2015, **54**, 7139; (*b*) D. Basu, S. Mazumder, J. Niklas, H. Baydoun, D. Wanniarachchi, X. Shi, R. J. Staples, O. Poluektov, H. B. Schlegel and C. N. Verani, *Chem. Sci.*, 2016, **7**, 3264.
18 See the ESI† for computational details.
19 R. S. Khnayzer, V. S. Thoi, M. Nippe, A. E. King, J. W. Jurss, K. A. El Roz, J. R. Long, C. J. Chang and F. N. Castellano, *Energy Environ. Sci.*, 2014, **7**, 1477.

